4-1-2015

Dynamical Precipitation Downscaling for Hydrologic Applications Using WRF 4D-Var Data Assimilation: Implications for GPM Era

Liao-Fan Lin
Georgia Institute of Technology

Ardeshir M. Ebtehaj
Georgia Institute of Technology

Rafael L. Bras
Georgia Institute of Technology

Alejandro N. Flores
Boise State University

Jingfeng Wang
Georgia Institute of Technology

Dynamical Precipitation Downscaling for Hydrologic Applications Using WRF 4D-Var Data Assimilation: Implications for GPM Era

LIAO-FAN LIN, ARDESHIR M. EBTEHAJ, AND RAFAEL L. BRAS

School of Civil and Environmental Engineering, Georgia Institute of Technology, Atlanta, Georgia

ALEJANDRO N. FLORES

Department of Geosciences, Boise State University, Boise, Idaho

JINGFENG WANG

School of Civil and Environmental Engineering, Georgia Institute of Technology, Atlanta, Georgia

(Manuscript received 17 February 2014, in final form 16 October 2014)

ABSTRACT

The objective of this study is to develop a framework for dynamically downscaling spaceborne precipitation products using the Weather Research and Forecasting (WRF) Model with four-dimensional variational data assimilation (4D-Var). Numerical experiments have been conducted to 1) understand the sensitivity of precipitation downscaling through point-scale precipitation data assimilation and 2) investigate the impact of seasonality and associated changes in precipitation-generating mechanisms on the quality of spatiotemporal downscaling of precipitation. The point-scale experiment suggests that assimilating precipitation can significantly affect the precipitation analysis, forecast, and downscaling. Because of occasional overestimation or underestimation of small-scale summertime precipitation extremes, the numerical experiments presented here demonstrate that the wintertime assimilation produces downscaled precipitation estimates that are in closer agreement with the reference National Centers for Environmental Prediction stage IV dataset than similar summertime experiments. This study concludes that the WRF 4D-Var system is able to effectively downscale a 6-h precipitation product with a spatial resolution of 20 km to hourly precipitation with a spatial resolution of less than 10 km in grid spacing—relevant to finescale hydrologic applications for the era of the Global Precipitation Measurement mission.

1. Introduction

Precipitation is an important component of global and regional hydrologic cycles. Since December 1997, the Tropical Rainfall Measuring Mission (TRMM) has been providing a wealth of spaceborne precipitation data. Among these, the TRMM Multisatellite Precipitation Analysis (TMPA) has provided 3B42 rainfall products at resolutions as fine as 0.25° × 0.25° in space and 3 h in time over the tropics, which covers 50°N–50°S (Huffman et al. 2007). The success of the TRMM has led to the Global Precipitation Measurement (GPM) mission, which consists of a core observatory and a complementary set of existing and new satellites that will be cross calibrated and operated as a constellation. As a successor of the TRMM, the GPM will provide spaceborne observations of precipitation with unprecedented resolutions that may reach up to 0.1° × 0.1° every 30 min in the future for a merged product that combines GPM core observations with measurements provided by other partner radiometers and infrared instruments (Hou et al. 2008, 2014).

From a hydrologic point of view, evolution of hourly high-intensity rain cells typically occurs at a spatial scale smaller than 10 km, which may not be fully resolved in satellite-based products. To enhance the resolution of satellite-based precipitation for hydrologic applications, such as flash flood forecasting and landslide prediction, numerous downscaling approaches have been studied. The two most common families of methodologies are dynamical and statistical downscaling approaches. Statistical methods consist of a large group of methodologies that use

Corresponding author address: Liao-Fan Lin, School of Civil and Environmental Engineering, Georgia Institute of Technology, 790 Atlantic Dr., Atlanta, GA 30332-0355.
E-mail: liaofan.lin@gatech.edu

DOI: 10.1175/JHM-D-14-0042.1

empirical multiscale statistical relationships, parameterized by observations or other environmental predictors, to reproduce realizations of multiscale precipitation fields (Fowler et al. 2007). This family of downscaling approaches is not typically capable of resolving the complex underlying dynamics of precipitation processes and is thus unable to produce realistic and sufficiently accurate precipitation at high spatiotemporal resolutions (Gutmann et al. 2012). On the other hand, dynamical downscaling approaches are computationally more demanding than their statistical counterparts (Hellstrom et al. 2001) but are able to resolve the inherent precipitation dynamics (Schmidli et al. 2007). In addition, the family of dynamical downscaling methods is also able to provide hydrometeorological variables (e.g., downward radiation, surface temperature, and surface wind speed) that are physically consistent with the downscaled precipitation and required by many hydrological models. To this end, this paper attempts to use a physically based mesoscale weather forecasting model together with a variational data assimilation (DA) scheme for producing high-resolution hourly precipitation products with a spatial scale of less than 10 km in grid spacing.

Data assimilation—a mathematical approach integrating observations into a dynamic model—is used to dynamically downscale satellite precipitation products with an atmospheric prediction system for hydrologic applications (Zupanski et al. 2011; Zhang et al. 2013). Together with data assimilation, dynamical downscaling approaches that use a physically based model can integrate satellite observations with underlying physics to spatially and temporally downscale coarse-scale precipitation data and other meteorological variables. To provide improved precipitation analysis, some studies have focused on the assimilation of precipitation into atmospheric models using variational data assimilation techniques. For example, the four-dimensional variational data assimilation (4D-Var) of precipitation has been implemented in operational regional climate models, including those of the Japan Meteorological Agency (JMA) and the Met Office of the United Kingdom (Bauer et al. 2011b). The 4D-Var technique has been shown to improve short-term (i.e., 1–3 days) precipitation forecasts (Tsuyuki 1996a,b, 1997; Zupanski and Mesinger 1995). Koizumi et al. (2005) used the JMA 4D-Var system to assimilate 1-h radar-based precipitation data at a spatial resolution of 20 km and found improved precipitation forecasts up to 18 h ahead. Mesinger et al. (2006) assimilated hourly precipitation observations into the North American Regional Reanalysis system, which provides 32-km spatial resolution products every 3 h, and demonstrated improvements in the precipitation analysis compared to the reference monthly observations. Furthermore, Lopez (2011) and Lopez and Bauer (2007) assimilated the National Centers for Environmental Prediction (NCEP) stage IV gauge-corrected radar precipitation into the global Integrated Forecasting System of the European Centre for Medium-Range Weather Forecasts (ECMWF) and found substantial improvement in the short-term (i.e., up to 12 h) precipitation forecasts.

As an alternative to direct assimilation of precipitation, the assimilation of satellite radiances into atmospheric models is also frequently used to improve precipitation forecasts. The assimilation of radiances, however, requires a radiative transfer model, which simulates radiances at the top of the atmosphere based on simulated atmospheric (and sometimes land) states. Compared to precipitation assimilation, radiance assimilation is more straightforward, partly because the nonzero and space–time continuous nature of radiances that better conform to the Gaussian assumption in data assimilation. However, radiance assimilation can be challenging because of the difficulty of resolving cloud water in an atmospheric data assimilation system. Bauer et al. (2006a,b) implemented a 1D + 4D-Var algorithm into the ECMWF system to assimilate radiances under rainy conditions, while Bauer et al. (2010) and Geer et al. (2010) used a 4D-Var algorithm to assimilate all-sky radiances. Zupanski et al. (2011), Zhang et al. (2013), and Chambon et al. (2014) used an ensemble data assimilation system to assimilate precipitation-affected radiances such as those from the Advanced Microwave Scanning Radiometer for Earth Observing System (AMSR-E), the TRMM Microwave Imager (TMI), and the Microwave Humidity Sounder (MHS) for improving precipitation forecasts and providing downscaled precipitation estimates relevant to the GPM products. Zhang et al. (2013) found that the precipitation forecasts can be improved by radiance assimilation, and this improvement becomes more pronounced when precipitation intensity decreases and the spatial scale of analysis coarsens. Chambon et al. (2014) showed that the radiance assimilation reduces the root-mean-square error (RMSE) of 2-day accumulated precipitation at a 9-km resolution by 8.1% and improves the correlation of spatial rainfall patterns from 0.57 to 0.63, when compared to the results without assimilating radiances.

The Weather Research and Forecasting (WRF) Model data assimilation (WRFDA) is an open-source system that has been widely used to improve precipitation forecasting. Because of the growing interest in the WRFDA system and associated community-based developments, the WRFDA system has been equipped with extensive capability to assimilate various types of observations. The WRFDA system has DA options such as three-dimensional variational data assimilation (3D-Var), 4D-Var, and hybrid

variational-ensemble DA that permit assimilating a wide range of observations including in situ measurements, Doppler radar reflectivity, precipitation, and radiances (Barker et al. 2012; Wang et al. 2013). For example, the 3D-Var assimilation of conventional ground-based data and radiance observations has been used for improving precipitation forecasts at various spatial resolutions (Ha et al. 2011; Ha and Lee 2012; Hsiao et al. 2012; Liu et al. 2012; Routray et al. 2010; Schwartz et al. 2012; Xu and Powell 2012).

This study uses version 3.4 of the WRF Model (see Skamarock et al. 2008) and the WRFDA system (Barker et al. 2004, 2012; Huang et al. 2009). Note that the WRFDA system is currently not fully capable of assimilating precipitation-affected radiances (Barker et al. 2012), and thus, we only focus on the assimilation of precipitation for our dynamical downscaling experiments using the 4D-Var module. Specifically, we first focus on assimilating a point-scale observation at a single site to shed light on the sensitivity of dynamical downscaling to precipitation assimilation. Afterward, in real case experiments, we study the impact of outlier removal and seasonality on dynamical precipitation downscaling. It is important to note that, unlike classic data assimilation studies, which focus on improving the forecast skills of a model, we use the WRF Model and the WRFDA system to improve the spatiotemporal resolution of remotely sensed rainfall observations. In this paper, we use an upscaled (20-km grid boxes) version of 6-h NCEP stage IV precipitation [see Lin and Mitchell (2005) for the original version of stage IV data] as a general surrogate for a coarse-scale remotely sensed precipitation product and compare the downscaled results with the reference stage IV data at a gridded spatial resolution of 9 km. Although the spatial scale of the surrogate input precipitation is chosen closely to the current TRMM 3B42 product, we assimilated 6-h precipitation to be consistent with the default assimilation window of the WRF 4D-Var system. It is worthwhile noting that Lopez (2011) reported that assimilating 6-h stage IV precipitation in their ECMWF system exhibited more improved analyses than assimilating 1- or 3-h precipitation. In addition, we need to note that the chosen surrogate precipitation may not be fully consistent with the envisaged future space–time resolution of the GPM products. However, as we use a physically based model for downscaling, the promising results of this attempt can be considered as a proof of concept for possible downscaling of GPM precipitation to the hydrologic scales of interest.

In summary, the main findings of this study are the following: 1) the proposed dynamical downscaling framework can effectively reproduce high space–time resolution data from coarse-scale remotely sensed precipitation measurements; 2) the approach can suppress false heavy rainfall forecasts in the final downscaled fields; and 3) the methodology can properly translate assimilated data from the coarse-resolution parent domain into the high-resolution child domain and resolve the small-scale rainfall variability of interest. The rest of the paper is organized as follows. Section 2 presents the numerical experiment setup. Section 3 shows the results of three experiments, and section 4 discusses conclusions and future research.

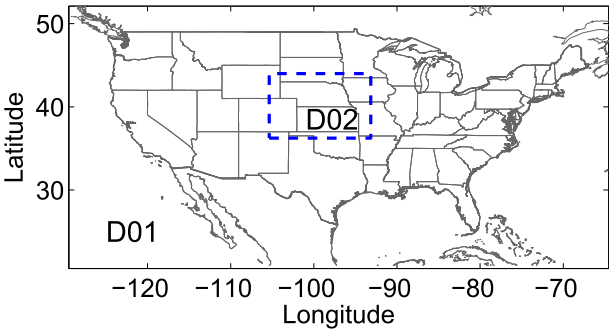

FIG. 1. Model domain configuration with an outer domain (D01) of 160 × 100 grids with a 36-km resolution and an inner domain (D02) of 121 × 101 grids with a 9-km grid resolution.

2. Model configurations and experiment design

This study configured the WRF Model with a nested domain as shown in Fig. 1, covering an outer 160 × 100 domain with a 36-km resolution and an inner 121 × 101 domain with a 9-km resolution. One-way nesting was used in order to support assimilation of coarse-scale precipitation and facilitate dynamical downscaling. The top pressure level of the experimental domain is set at 50 hPa with 40 vertical levels extending to the ground surface. The WRF Model physics options used in this study include schemes of the WRF single-moment 3-class microphysics (Hong et al. 2004), the Rapid Radiative Transfer Model for longwave radiation (Mlawer et al. 1997), the Dudhia shortwave radiation (Dudhia 1989), the MM5 similarity surface layer, the Noah land surface model (Chen and Dudhia 2001), the Yonsei University (YSU) planetary boundary layer (Hong et al. 2006), and the Kain–Fritsch cumulus parameterization (Kain and Fritsch 1990).

Figure 2 shows our experiment flowchart. We conducted three sets of experiments over three different periods: 1) a synthetic experiment that investigates the assimilation of a point-scale precipitation observation from 1800 UTC 10 June to 0000 UTC 11 June 2009, 2) winter experiments on 11 February 2009, and 3) summer experiments from

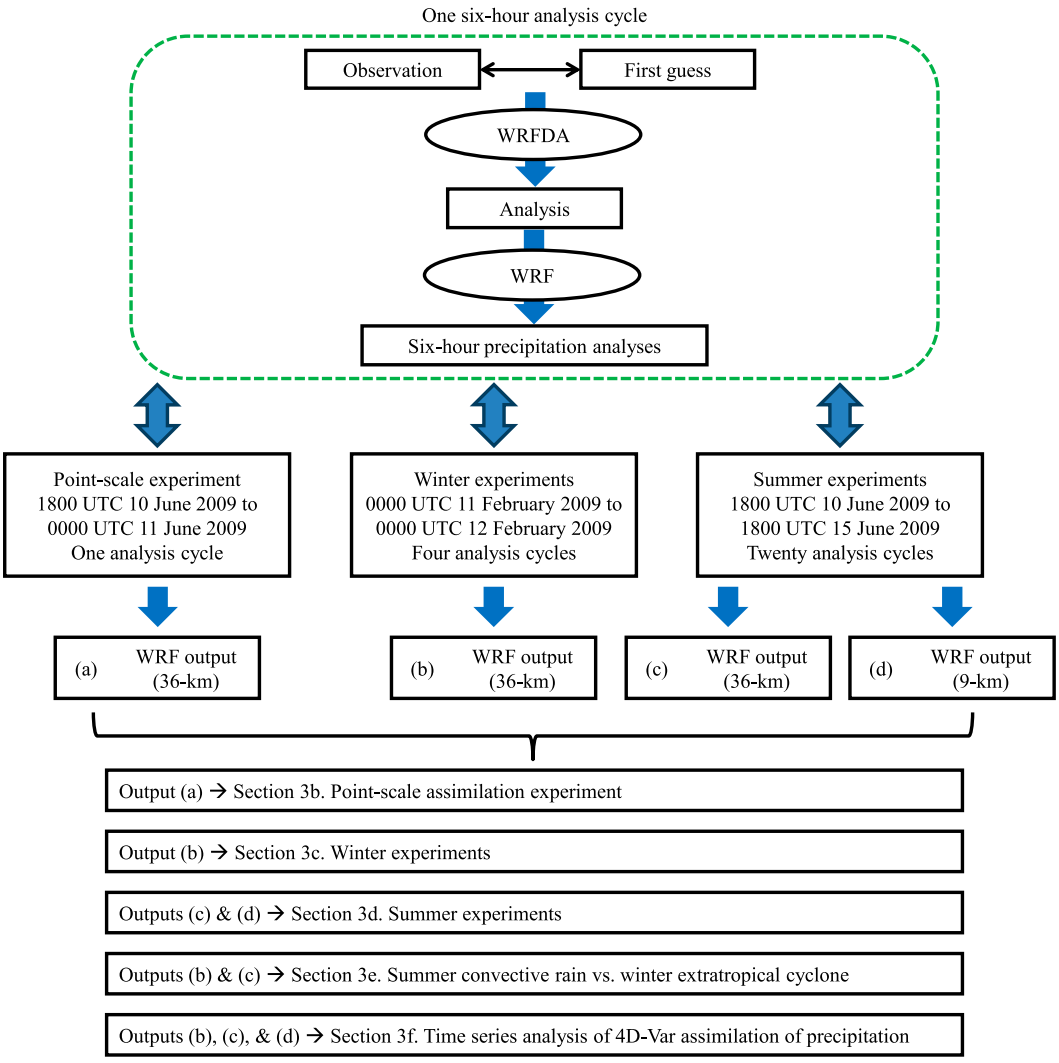

FIG. 2. Flowchart of this study.

1800 UTC 10 June to 1800 UTC 15 June 2009. In these experiments, we use a 6-h analysis cycle, and thus, each set of experiments contains 1, 4, and 20 analysis cycles, respectively. The purpose of the point-scale experiment is to understand the sensitivity of precipitation assimilation in the WRFDA system. In both the winter and summer experiments, we investigate the impact of the built-in quality-control option on our downscaling approach. In contrast to the winter experiments, the summer experiments are important for evaluating the ability of our dynamical downscaling approach to reproduce precipitation at fine space–time resolutions during convective events.

For all WRFDA experiments, we specify several general settings, including the specifications of the assimilation domain, first guesses, cycling mode, and background error covariance estimation. First, the DA process is employed only on the outer domain as all experiments use one-way nesting. Second, all experiments use the NCEP Final (FNL) operational global analysis dataset with 6-h, $1° \times 1°$ resolutions to generate first guesses or "background states." Third, this study designs a noncycling process, in which the first guesses are generated based on NCEP FNL data, while the first guesses in the cycling mode are typically obtained from short-range (typically 1–6 h) forecasts (Skamarock et al. 2008, p.88). Fourth, the control variables (CVs) in the WRFDA system are streamfunction, unbalanced potential velocity, unbalanced temperature, unbalanced surface pressure, and pseudorelative humidity (Barker et al. 2004). For all cases, the background error covariance was obtained by computing the average difference between 12- and 24-h forecasts valid at the same time using the National Meteorological Center (NMC)

method (Parrish and Derber 1992). The NMC method generates domain-dependent, static background error covariance matrices, referred to as CV5 in the WRFDA system.

In addition to the above general WRFDA settings, we have two specific settings for the WRF 4D-Var assimilation of precipitation. These include an optional quality control for innovations (i.e., observation minus background) and constructing the thinning mesh. First, in some experiments, we employ the quality control of innovation (QCI) to reject outlier observations for which the innovation exceeds 5 times the specified observation error, which is set to 2 mm $(6\,\mathrm{h})^{-1}$ in all experiments. Moreover, we use a 20-km thinning mesh to reduce overlapping observations at a given spatial resolution.

To understand how point-scale rainfall assimilation affects WRF primary state variables, we first conduct the 4D-Var synthetic experiment involving assimilation of only one perturbed precipitation observation at an arbitrary location (34.27°N, 98.16°W). The selected location is associated with approximately 26 mm of accumulated precipitation over a 6-h period in the open-loop forecasts, which represent WRF forecasts without any assimilation in this study. As is evident, the position of this point is carefully selected, as it is surrounded by a strong precipitation forecast. Using the explained experiment settings, we assimilate a synthetic observation, which is generated by adding a small (1 mm) positive increment to the 6-h precipitation forecast at the selected location.

The winter and summer seasons are characterized by different precipitation patterns and mechanisms. The winter experiments focus on a large-scale extratropical cyclone over the United States dominated by stratiform precipitation that lasted for almost 1 day over our study domain. On the other hand, the summer experiments include strong and local convective storms over the 5 days. Since the resolution of the assimilated precipitation does not capture the local nature of these intense summertime convective events, recovery of these small-scale, high-intensity activities using the dynamical downscaling approach is challenging. To study the effects of large innovations in dynamical downscaling, we also investigate two scenarios, with and without the QCI in both winter and summer experiments.

3. Results

a. Statistical basis for the comparison of experiments

We use three main statistical metrics to quantify the performance of the proposed dynamical downscaling approach, namely, 1) RMSE, 2) mean absolute error (MAE), and 3) correlation ρ between modeled (downscaled) and observed (reference) precipitation. The RMSE is defined as

$$\mathrm{RMSE} = \sqrt{\frac{1}{nm}\sum_{i=1}^{n}\sum_{j=1}^{m}[R_M(i,j) - R_O(i,j)]^2}, \quad (1)$$

where R_M and R_O are the m-by-n modeled and observed precipitation 2D fields, respectively. The MAE is defined as follows:

$$\mathrm{MAE} = \frac{1}{nm}\sum_{i=1}^{n}\sum_{j=1}^{m}|R_M(i,j) - R_O(i,j)|. \quad (2)$$

Note that the RMSE markedly penalizes large anomalies compared to the MAE, which uniformly penalizes all anomalies. Furthermore, to explore the predictive skill of the proposed dynamical downscaling approach, we also use normalized differences between the performance metrics of the open-loop and 4D-Var results, as follows:

$$\frac{\mathrm{RMSE}_{\text{open loop}} - \mathrm{RMSE}_{\mathrm{DA}}}{\mathrm{RMSE}_{\text{open loop}}} \quad (3)$$

and

$$\frac{\mathrm{MAE}_{\text{open loop}} - \mathrm{MAE}_{\mathrm{DA}}}{\mathrm{MAE}_{\text{open loop}}}. \quad (4)$$

To evaluate the correlation between the downscaled and reference precipitation fields, the classic Pearson cross-correlation coefficient (i.e., ρ) is used.

b. Point-scale assimilation experiment

Figure 3 shows the analysis increments (i.e., analyses minus the first guesses) of zonal wind, meridional wind, surface dry air mass pressure, surface pressure, potential temperature, and specific humidity at the lowest model level. These figures are meant to demonstrate how a small (1 mm) perturbation in the assimilated precipitation propagates into the WRF state variables via the 4D-Var algorithm. As a result of assimilation, maximum analysis increments are $3.28 \times 10^{-4}\,\mathrm{m\,s^{-1}}$ for zonal wind, $4.25 \times 10^{-4}\,\mathrm{m\,s^{-1}}$ for meridional wind, 0.24 Pa for surface dry air mass pressure, 0.031 Pa for surface pressure, $2.7 \times 10^{-4}\,\mathrm{K}$ for potential temperature, and $2.01 \times 10^{-6}\,\mathrm{kg\,kg^{-1}}$ for specific humidity. While the maximum absolute increments are small, it is interesting to note that the 4D-Var algorithm in the WRFDA system affects the primary state variables over a relatively large area, which may be partly due to the smoothing effects of the background error covariance. Unlike other state variables with widespread increments, the specific humidity shows a limited spatial spread.

Despite the fact that the small magnitude of the assimilated perturbation did not substantially affect the magnitude of WRF primary state variables, we found that

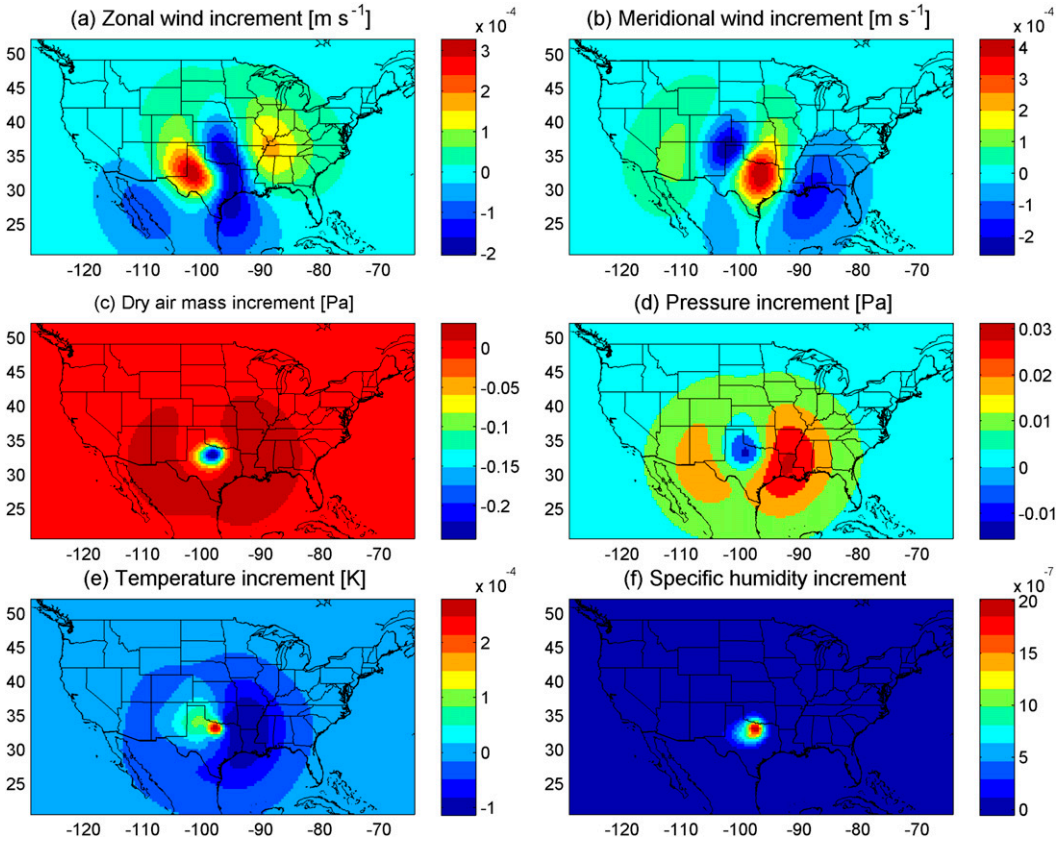

FIG. 3. The increments of several variables defined as the analyses minus the first guesses at the lowest model level from the synthetic experiment of the 4D-Var assimilation of a 6-h accumulated precipitation observation at a single site: (a) zonal wind (m s^{-1}), (b) meridional wind (m s^{-1}), (c) surface dry air mass pressure (Pa), (d) surface pressure (Pa), (e) potential temperature (K), and (f) specific humidity (kg kg^{-1}).

the influence on the analysis rainfall is substantial. Figure 4a shows the open-loop forecasts of the rainfall field from 1800 UTC 10 June to 0000 UTC 11 June 2009 covering the contiguous United States, while Fig. 4b shows the 6-h accumulated rainfall analyses minus the open-loop forecasts. A total of 116 pixels out of 160 000 pixels have 6-h deviation (analysis minus forecast) greater than 1 mm with the maximum value of 9.17 mm. Note that those pixels usually correspond to rainy pixels of the open-loop forecast. After 6 h of nonlinear model integration, the small rainfall perturbation not only is propagated throughout the entire domain but also causes a significant deviation much larger than the perturbation itself over a significant surrounding area. The results clearly suggest that the 4D-Var rainfall analysis might be markedly sensitive to assimilated rainfall observations.

c. *Winter experiments*

In this section, we focus on the winter experiments and devote special attention to comparing the results of multiple assimilation scenarios. As the NCEP stage IV data are only available over land, we selected a rectangular region of interest that corresponds to 66 × 41 grid cells (2706 pixels total) within the outer domain. The winter experiments consist of the following three scenarios:

1) OpL, which is the open-loop WRF forecast without DA;
2) *P*-noQCI, which is assimilation of 20 km, 6-h accumulated precipitation *P* using the 4D-Var algorithm without the QCI; and
3) *P*-QCI, which is the same as *P*-noQCI but with the QCI.

Figure 5 shows 1-day precipitation accumulations from the reference NCEP stage IV data, the open-loop forecasts, and the two precipitation assimilation scenarios. The analysis fields show a good visual agreement with the reference field, which is also well reflected in the computed statistical metrics (see Fig. 5d). Moreover, the improvement is more significant when we use the built-in QCI. Note that, in each analysis cycle during the 1-day experiments, the *P*-noQCI scenario used the entire 29 996 precipitation data points within the outer domain, while the *P*-QCI experiment filtered out 431,

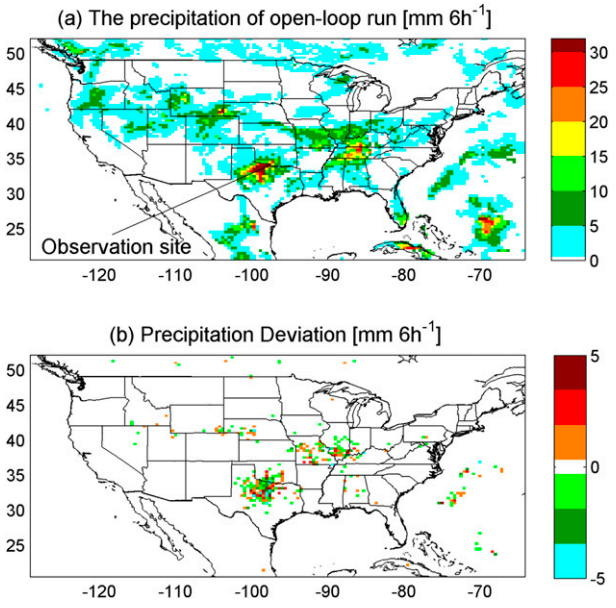

FIG. 4. Precipitation analysis and forecast [mm $(6\,\mathrm{h})^{-1}$] in the point-scale assimilation experiment from 1800 UTC 10 Jun to 0000 UTC 11 Jun 2009. (a) The 6-h accumulated precipitation of the open-loop experiment. (b) The deviation of 6-h accumulated precipitation computed as the precipitation of the DA experiment minus that of the open-loop experiment with a constrained scale from -5 to 5 mm $(6\,\mathrm{h})^{-1}$.

444, 279, and 338 data points in four analysis cycles, respectively. About 1% of the observations is removed in the analysis cycle and ultimately leads to a significant improvement in the precipitation analysis. Note also that, although *P*-noQCI leads to a close visual agreement with the reference data, the quantitative improvements are marginal, compared to the OpL scenario. In contrast, the *P*-QCI scenario shows the best RMSE (4.98 mm) and MAE (2.43 mm), which are equivalent to 29% and 28% relative improvements, respectively. This finding suggests that the removal of outliers can be a key element for successful implementation of the proposed dynamical downscaling via precipitation assimilation during the winter.

d. Summer experiments

In this section, we study the performance of dynamical downscaling for the summer experiments over both 36- (outer domain) and 9-km (inner domain) resolutions. Figure 6 shows the 5-day precipitation accumulations at the 36-km resolution for the same scenarios described in section 3c. The 4D-Var with the QCI scenario shows the most improved downscaled precipitation (Fig. 6d), while the 4D-Var without the QCI scenario shows significant overestimation (Fig. 6c). When compared to the reference dataset and OpL forecasts, the assimilation with the QCI scenario markedly improves the spatial patterns of precipitation analyses. For instance, the *P*-QCI scenario captures a band of rainfall that extends from northeastern Colorado through Kansas, northern Oklahoma, and northern Arkansas to northern Georgia, while the OpL scenario does not. In addition, the *P*-QCI scenario produced lower-intensity rainfall around Indiana, leading to a closer agreement with the reference data. Statistics of the 5-day precipitation accumulations also confirm that the 4D-Var assimilation with the QCI can substantially improve the spatial distributions of

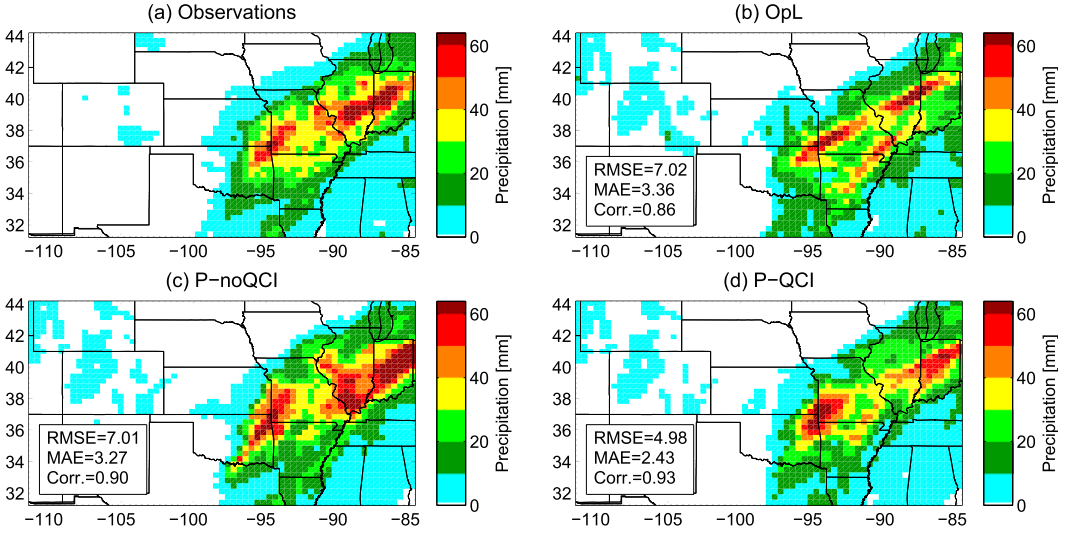

FIG. 5. The 1-day accumulated precipitation (mm) at the 36-km resolution for the winter experiments: (a) reference data from NCEP stage IV precipitation observations, (b) OpL, (c) *P*-noQCI, and (d) *P*-QCI. The RMSE (mm day^{-1}), MAE (mm day^{-1}), and ρ of modeled and observed precipitation are reported in (b)–(d).

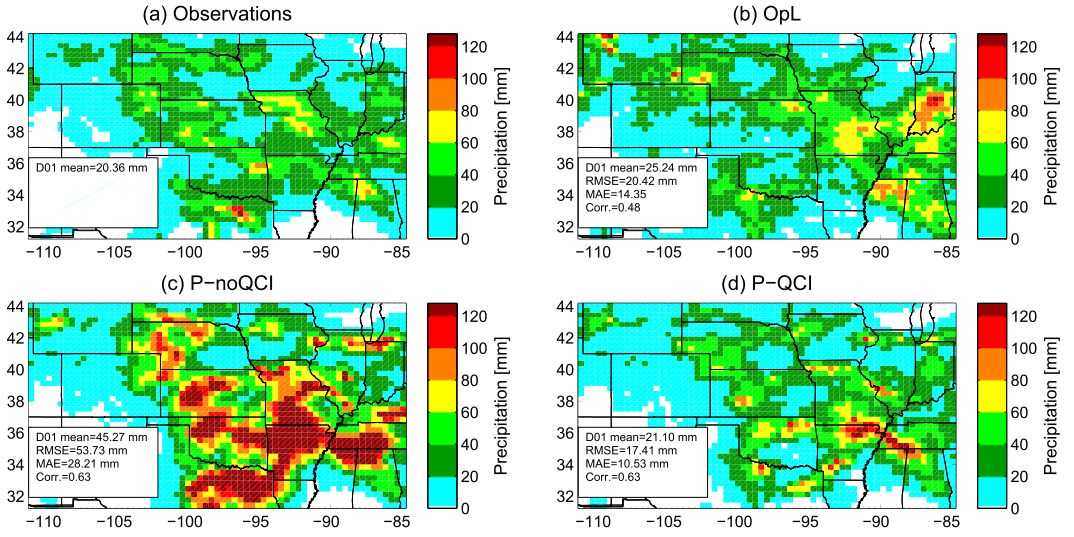

FIG. 6. The 5-day surface accumulated summer precipitation (mm) from the outer domain from 1800 UTC 10 Jun to 1800 UTC 15 Jun 2009: (a) reference data from NCEP stage IV precipitation observations, (b) Opl, (c) *P*-noQCI, and (d) *P*-QCI. The domain means are expressed in (a)–(d), while the RMSE, MAE, and ρ of modeled and observed precipitation are reported in (b)–(d).

precipitation. However, as is apparent, the assimilation experiment produces too much precipitation over northeastern Arkansas and western Tennessee. In addition to 5-day accumulations, we also compare the hourly domain means of the reference data with those of the *P*-QCI and the OpL scenarios at the 36-km resolution over the study region introduced in section 3c (Fig. 7). The results demonstrate that the hourly domain means of the *P*-QCI scenario are closer to those of the reference data than those for the OpL forecasts (Figs. 7a,b), showing the effectiveness of the QCI in our dynamical downscaling approach. In the sections below, we will only analyze the winter and summer assimilation experiments using the QCI.

The results for a selected region of interest in the inner domain (101 × 81 pixels at 9-km resolution) are shown in Fig. 8, which compares 5-day precipitation accumulations from the 4D-Var and the open-loop experiments with the reference data. This region excludes a 10-grid space of each side of the inner domain for convenience of analysis and to avoid any boundary effect. A closer scrutiny of Fig. 8 clearly shows that the dynamical downscaling approach improves the estimation of rainfall spatial distribution. In particular, four distinct features confirm that the 4D-Var experiment outperforms the open-loop experiment. First, a rainband from about 42°N, 104°W to 37°N, 97°W (a white-line irregular shape in Fig. 8) is captured by the 4D-Var experiment, which is in agreement with the reference data, but not captured well by the open-loop experiment. Second, along latitude 39°–40°N and within longitude 95°–99°W, the open-loop experiment predicted heavy rain of 40–80 mm, which is corrected with the data assimilation. Third, the WRF 4D-Var system successfully recovers a narrow strip with heavy precipitation along latitude 40°N and within longitude 95°–96°W (a white-line rectangle), which is missing in the open-loop experiment. Finally, all the statistics, the domain means, the RMSE, the MAE, and the correlation demonstrate that the WRF 4D-Var assimilation produces precipitation analyses in closer agreement with the reference data than the open-loop experiment.

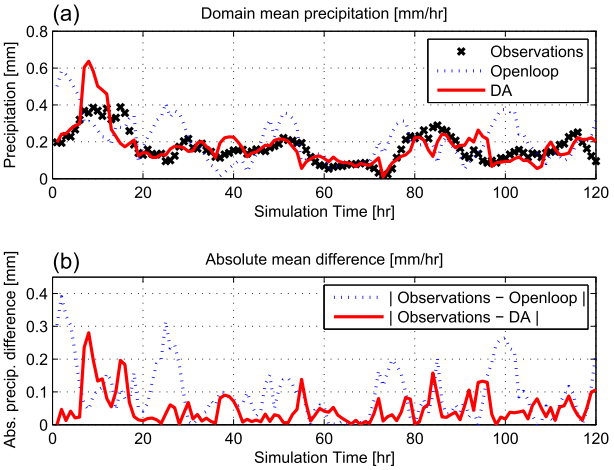

FIG. 7. The comparison of the domain means of hourly observed summer precipitation, the open-loop, and the DA experiments from the outer domain from 1800 UTC 10 Jun to 1800 UTC 15 Jun 2009. (a) Domain means and (b) the absolute value of the difference between the domain means of the reference data and open-loop forecasts and those between the reference data and the 4D-Var analyses.

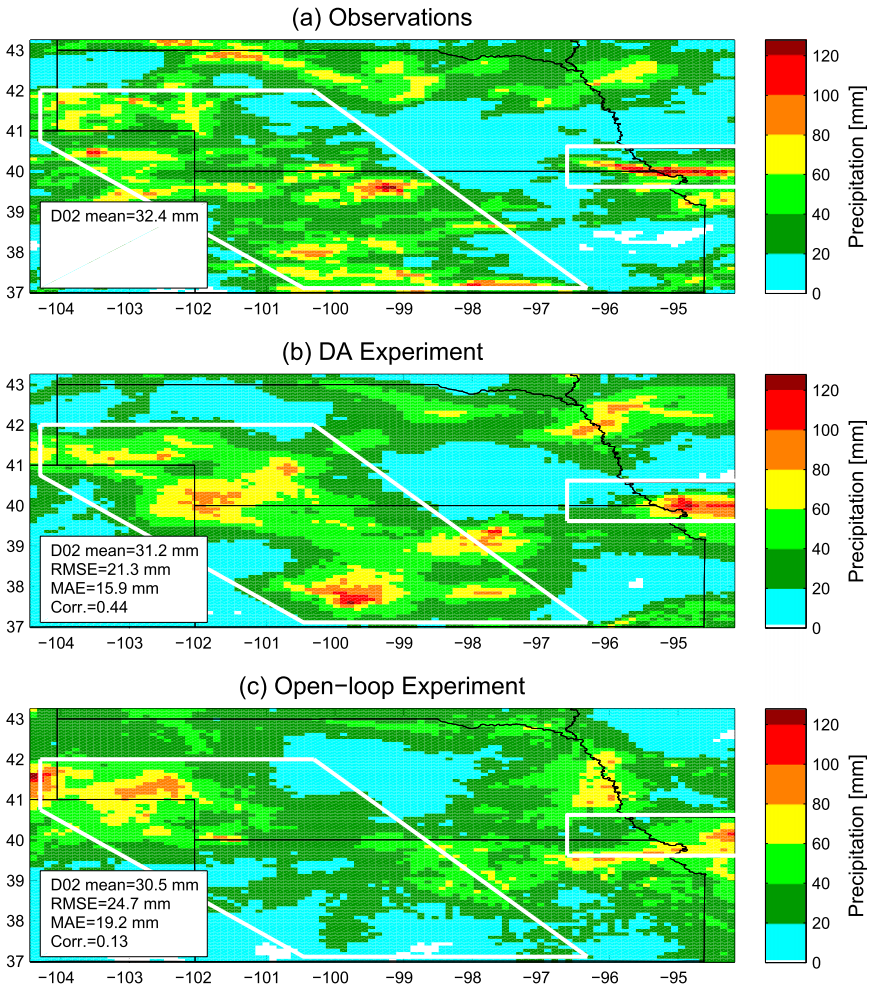

FIG. 8. The 5-day surface accumulated precipitation (mm) from the inner domain of the summer experiments from 1800 UTC 10 Jun to 1800 UTC 15 Jun 2009: (a) NCEP stage IV precipitation data, (b) 4D-Var experiment, and (c) open-loop experiment. The domain means are reported in (a)–(c). The RMSE, MAE, and ρ are computed between the modeled accumulated precipitation and observed data. The white-line regions are described in section 3d.

For each pixel within the region of interest in the inner domain, Fig. 9 compares the MAEs, correlations, and RMSEs among forecasts, analyses, and the reference data obtained from the hourly rainfall time series over the entire 8181 pixels. Figure 9a shows the MAE for the 4D-Var and open-loop experiments. A total of 60% of the MAE values fall below the diagonal line, indicating that the dynamical downscaling with 4D-Var performed better than the open-loop forecasts in 60% of pixels. For the correlation coefficients, Fig. 9b shows that the outperformance of 4D-Var over the open-loop experiment is even stronger, as 66% of the points fall above the diagonal line. The RMSE also shows that 55% of the pixels in the 4D-Var experiment have a better performance than the open-loop experiment. Note that the above assimilation experiments were only performed in the outer domain, and analysis outputs from the outer domain were used as the initial and lateral boundary conditions for the inner domain. Therefore, we observed that assimilation in the outer domain (36-km grids) produces improved initial and lateral boundary conditions for the inner domain (9-km grids) that ultimately lead to high-resolution and improved estimates of precipitation.

e. Summer convective rain versus winter extratropical cyclone

The purpose of this comparison is to understand the performance of the proposed dynamical downscaling approach for different seasons and rainfall mechanisms. The performance of assimilating 6-h accumulated precipitation in each DA analysis cycle of the 1-day winter experiments is compared with that of the 5-day summer

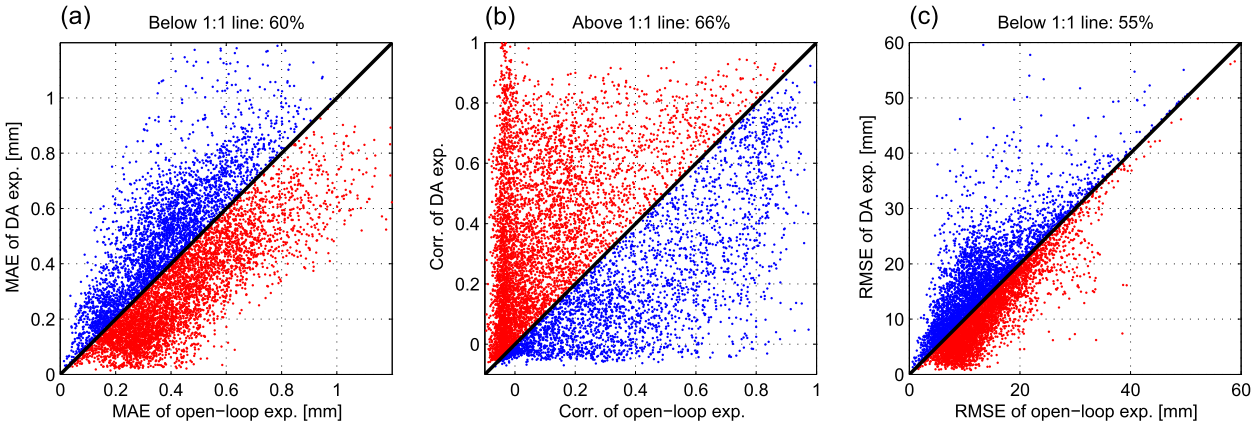

FIG. 9. The comparison of the (a) MAE, (b) ρ, and (c) RMSE of hourly precipitation for each grid of the open-loop experiment vs the DA experiment over the inner domain in the summer experiments. Higher density of the red dots compared to the blue dots shows that the 4D-Var experiment outperforms the open-loop experiment.

experiments over the region of interest at the outer domain resolution. As mentioned in section 2, the winter experiments are associated with an extratropical cyclone while the summer experiments consist of many convective storms. Figure 10 shows the correlation between the modeled and the observed precipitation and the predictive skill measured by RMSE and MAE, respectively, for every 6-h analysis cycle in both summer and winter experiments. For the winter experiments, the average correlation between the open-loop forecasts and the reference data is higher than that between the 4D-Var analyses and reference data from the summer experiments (Fig. 10a). This shows that the precipitation forecasts for the winter, even without using data assimilation, are in closer agreement with the reference data than the corresponding data assimilation experiment in the summer. It is reported in Fig. 10 that assimilation of precipitation increases the correlation between model output and reference data on average by 0.19 for the summer and 0.13 for the winter. In other words, data assimilation improves the summertime precipitation analyses more than the wintertime in terms of correlation. However, the end results are closer to the reference data in the winter because of better quality of the open-loop forecasts during the winter.

In addition, the skill measured by RMSE is relatively consistent for the analysis cycles during the winter but varies substantially and degrades sometimes during the summer. Figure 10b shows the skills measured by RMSE for the winter and summer experiments are 34% and 3%, respectively. Since RMSE penalizes large errors substantially, the poor summer skill may be due to over- or underestimation of localized extreme precipitation intensities by the data assimilation scheme. This suggests that in a convection dominant regime, precipitation extremes may not be well captured by the employed data assimilation system. Surprisingly, the skill of the 4D-Var measured by MAE shows an increase in skill of on average 31% and 29% for the winter and summer experiments, respectively (Fig. 10c). While both the summer and winter experiments have similar average MAE, the improvement in downscaled precipitation exhibits more spatial variability during the summer than winter. Note that the second analysis cycle in the summer experiment is associated with a large degradation in RMSE and MAE, and the sixteenth analysis cycle shows a large degradation measured by RMSE while no degradation measured by MAE.

Figure 11 shows 6-h precipitation of assimilation cycles 1, 2, 3, and 16 from the summer experiments, while Fig. 12 shows 6-h precipitation of cycles 1–4 from the winter experiments. These figures give more detail of the impact of nonassimilated observations due to the QCI. As discussed previously, cycles 2 and 16 in the summer experiments do not exhibit good assimilation skill as measured by RMSE (Fig. 10b). Figures 11j and 11l show where the WRF 4D-Var system significantly overestimates precipitation in comparison to the reference data in Figs. 11f and 11h, respectively, which is the major source of large RMSE. Note that this region is mainly dominated by convective activity for which its spatial extent is largely estimated correctly, but its precipitation intensities are overestimated by the 4D-Var algorithm. This situation happens much more frequently in the summer than in the winter, mainly because 1) the difference between the observed and forecasted precipitation can be very large for the cases of convective rainfall events, and thus the observations may not be used in the DA experiment because of the QCI, and 2) the prescribed background error covariance can affect model states at

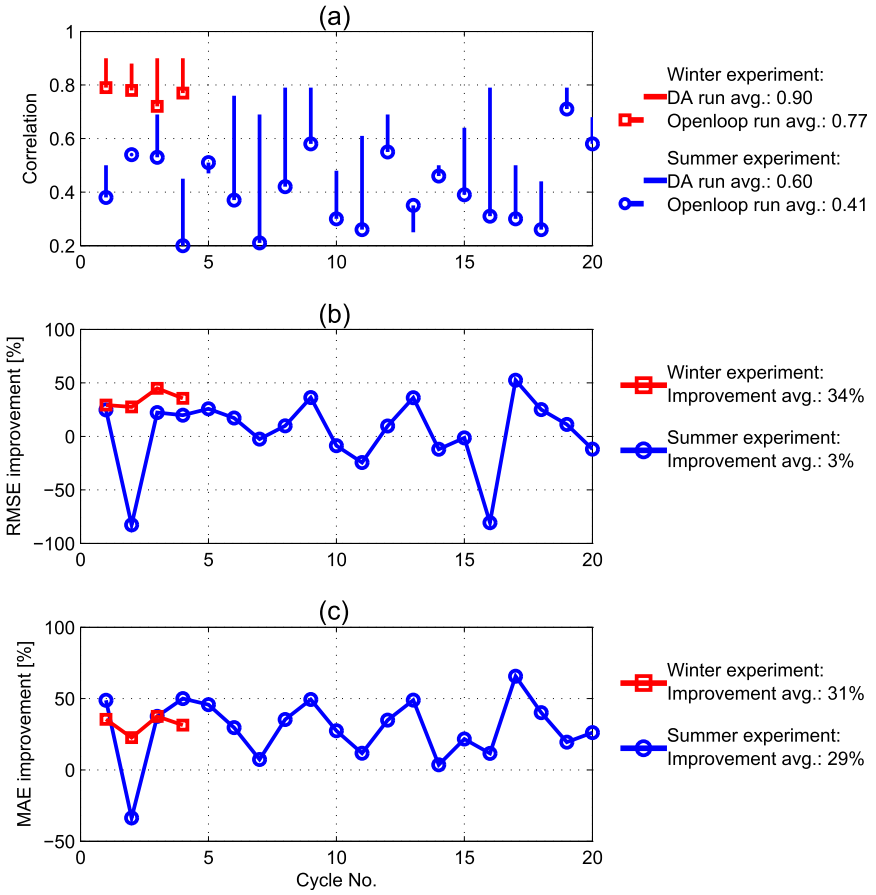

FIG. 10. The statistics of the summer experiments (blue) and the winter experiments (red): (a) ρ between the 6-h accumulation of modeled and observed precipitation. The hollow circles and squares represent the ρ between the open-loop experiment and reference data. The other end of each line without a circle or a square represents the ρ between the DA experiment and reference data. (b),(c) The skill of modeling improvement in terms of RMSE and MAE, respectively.

a large spatial extent and may not benefit our proposed downscaling approach in capturing local precipitation extremes. The gray regions in northern Texas (Fig. 11b) and in Tennessee, Alabama, and Mississippi (Fig. 11d) are those areas where the observations are considered to be outliers in the QCI module and have not been used in the 4D-Var algorithm. Notice that these areas are typically surrounded by relatively large positive innovations in the studied convective dominant storm. As a result, the positive innovations and the large spatial footprint of the background error covariance typically lead to overestimation in those gray regions where no observations are assimilated to properly constrain the overestimation through the cost function of 4D-Var algorithm. In contrast, since winter open-loop forecasts are relatively accurate, the innovation magnitudes mainly remain within the acceptable bounds of the QCI. Thus, the WRFDA typically assimilates a major fraction of heavy precipitation observations within the storm. In Figs. 12a–d, it can be seen that the wintertime 4D-Var assimilates relatively more areas of heavy precipitation observations than that of the summertime experiments and thereby do not exhibit significant overestimation. This problem further manifests itself in summertime experiments when open-loop forecasts completely miss the observed small-scale convective cells. In this case, the 4D-Var with the QCI typically ignores the observations and totally misses information content of important convective precipitation features of the storm. Figure 11g shows a small but heavy precipitation patch in Texas that was observed but not assimilated (Fig. 11c). Therefore, over this heavy rainfall patch, data assimilation does not alter the precipitation analyses significantly compared to the forecasts (Fig. 11o), and the analysis rainfall intensities remain almost unchanged (Fig. 11k). However, it can be seen that the WRF 4D-Var system effectively reduces

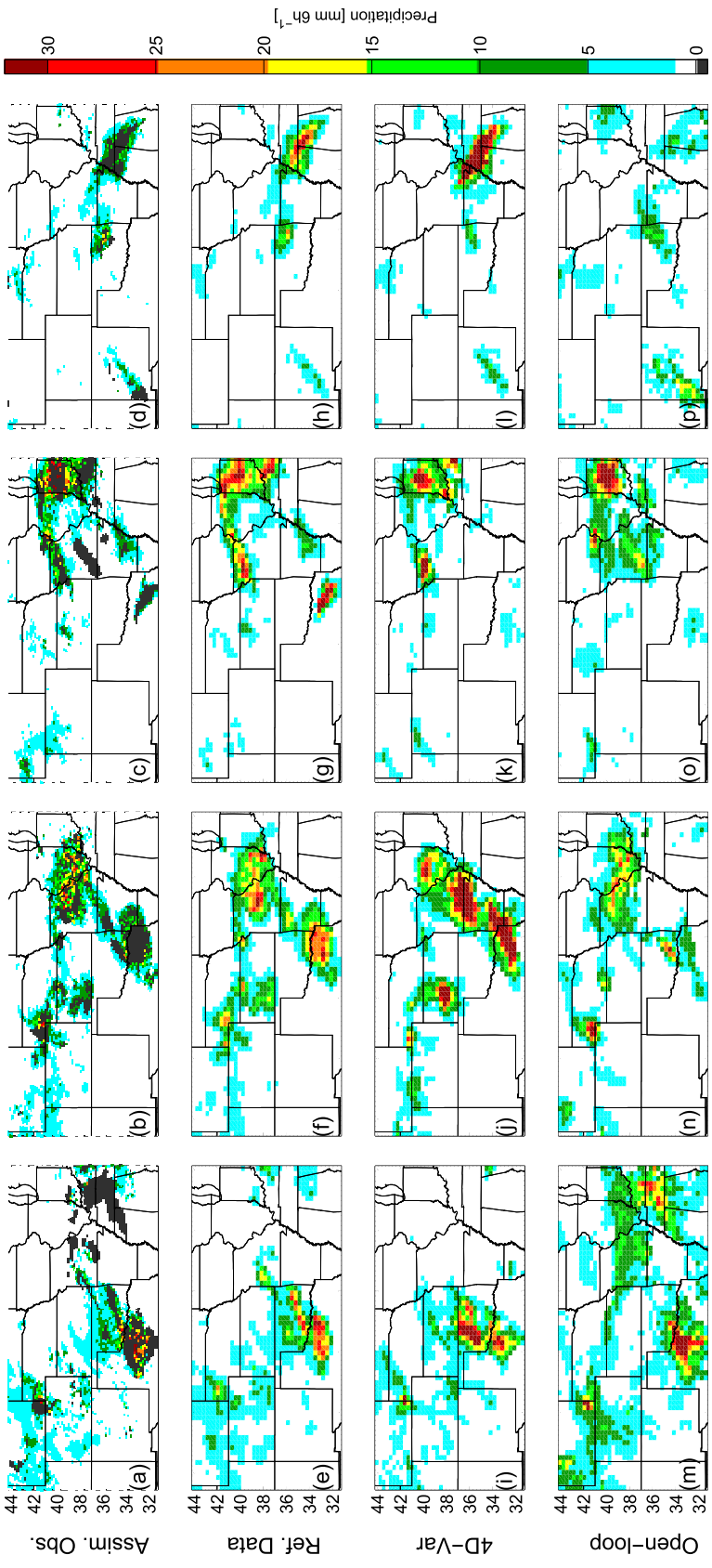

FIG. 11. The 6-h precipitation (mm) of cycles 1, 2, 3, and 16 from the summer experiments using the QCI. (a)–(d) The assimilated observations at 20-km resolution of the four selected cycles, respectively. Those gray regions denote the locations where observations were filtered by the QCI and not assimilated. (e)–(h) The reference data at 36-km resolution. (i)–(l) The 4D-Var analyses with using the QCI at 36-km resolution. (m)–(p) The open-loop forecasts at 36-km resolution.

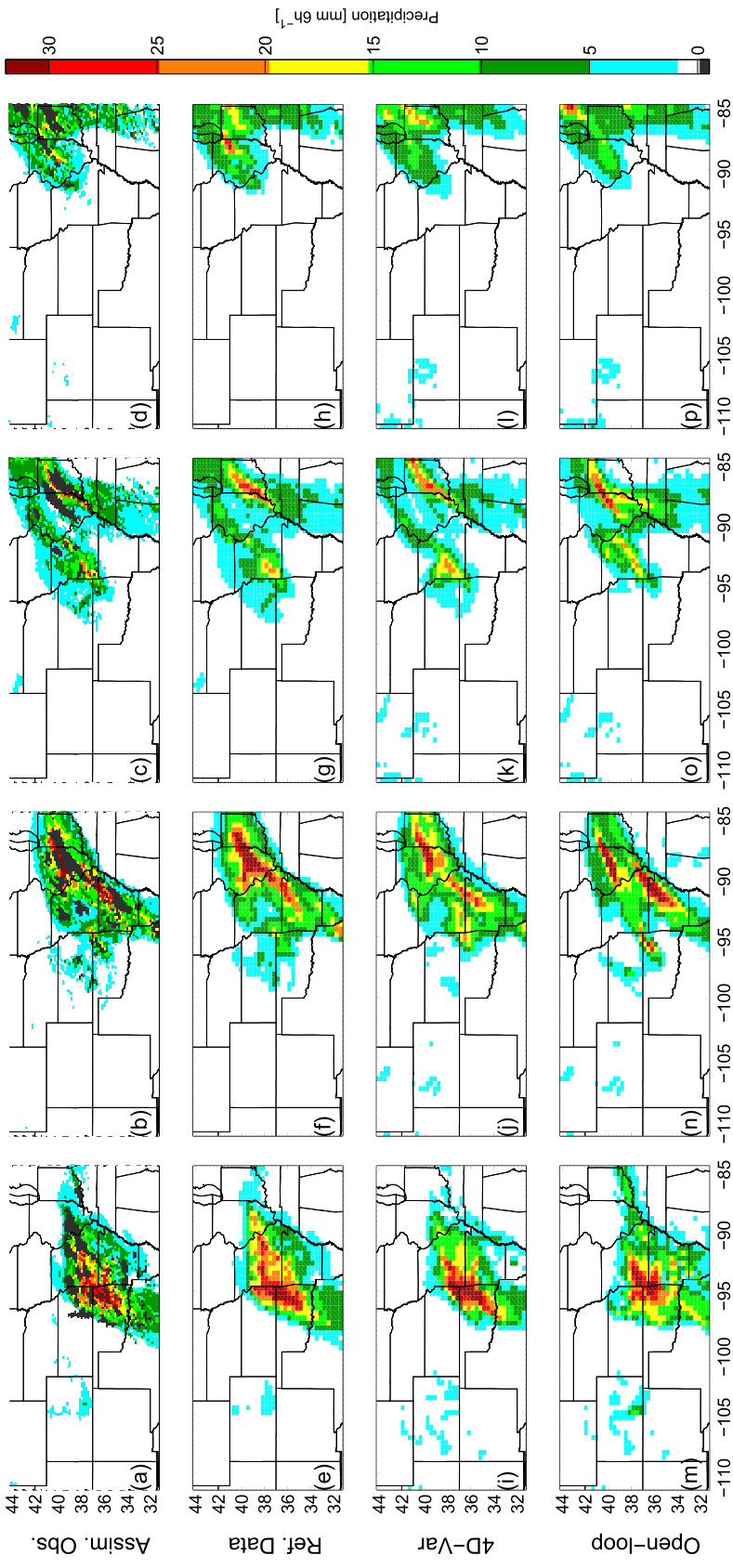

FIG. 12. As in Fig. 11, but for cycles 1, 2, 3, and 4 from the winter experiments.

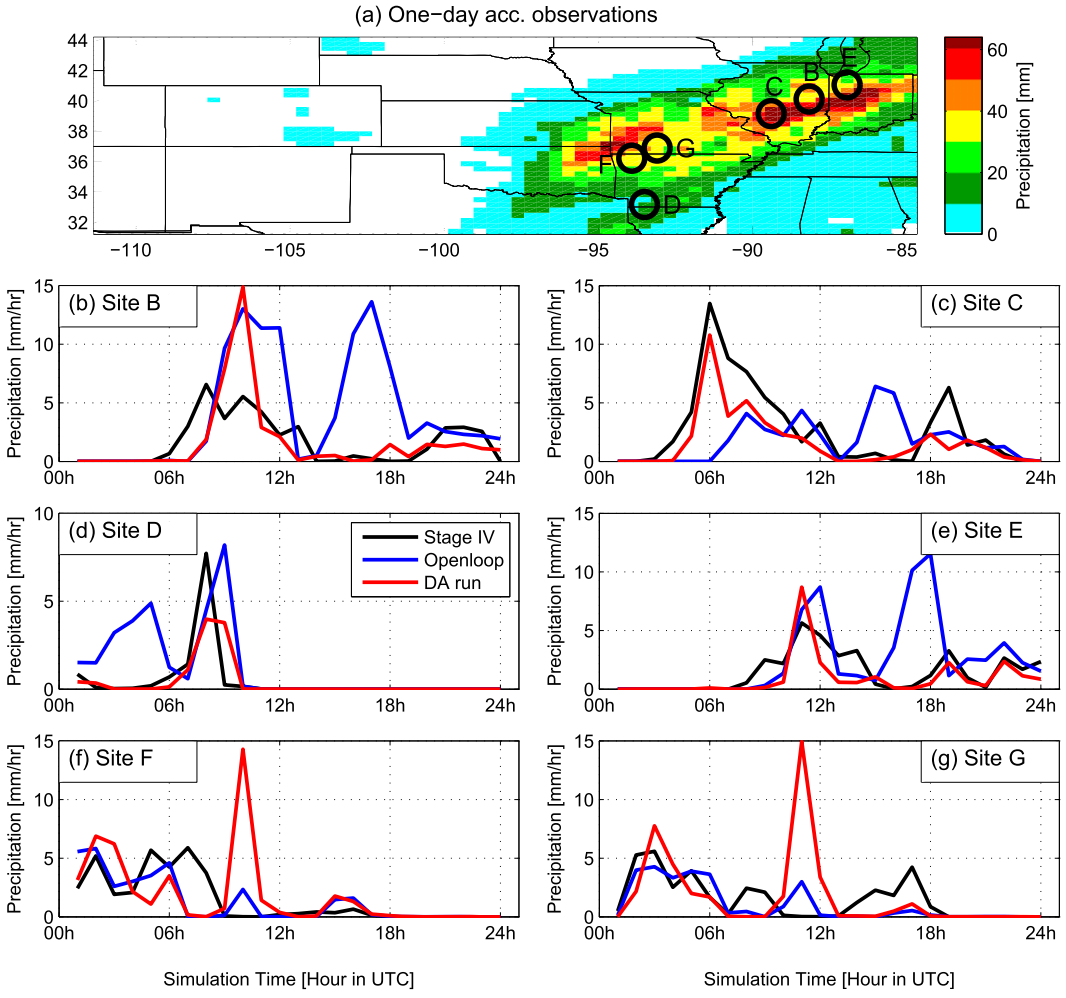

FIG. 13. (a) Observed accumulated precipitation and the locations of selected sites (black circles) from the outer domain (36-km resolution) of the 1-day winter experiments. (b)–(g) The time series of hourly precipitation of stage IV reference data (black), the open-loop experiment (blue), and the 4D-Var experiment (red) for sites B–G, respectively.

precipitation errors when the open-loop forecasts produce heavy rain over the areas where the observations suggest no rain or light rain. Figure 11m shows heavy rain forecasts within longitudes 85°–95°W, while we see little or very light rainfall in Figs. 11e and 11i. Even though Fig. 11a has a gray region of nonassimilated observations, the assimilated observations surrounding the gray region ultimately reduce forecast errors significantly and lead precipitation analyses in a good agreement with the reference data. Therefore, the QCI seems very effective when the open-loop experiment falsely predicts rainfall, while giving rise to misleading results when the open-loop forecasts miss observed localized precipitation events.

f. Time series analysis of 4D-Var assimilation of precipitation

In this section, we focus on understanding how the 4D-Var scheme impacts wintertime and summertime precipitation analyses at hourly and pixel scales (the smallest simulation unit) within the experimental domain. We select a set of pixels over the study domain where the accumulated precipitation exceeds certain thresholds and discuss the temporal aspects of the proposed dynamical downscaling in those locations.

1) TIME SERIES OF 1-DAY WINTER EXPERIMENTS (36-KM RESOLUTION)

Figure 13a shows the 1-day accumulated precipitation from the reference data and the location of six selected sites for hourly time series analysis. The precipitation time series at the sites are shown in Figs. 13b–g with the corresponding statistics presented in Table 1. To study the effects of the dynamical downscaling approach on capturing high-intensity precipitation over the studied domain, we select six individual locations based on the following criteria: 1) sites B and C exhibit accumulated

TABLE 1. The statistics of selected sites in Figs. 13–15. Units are millimeters.

	B	C	D	E	F	G
1-day experiments for the winter (D01)						
Accumulated precipitation (OBS)	39	65	11	34	33	34
Accumulated precipitation (OpL)	98	41	29	59	30	25
MAE (DA vs OBS)	1.47	1.28	0.38	0.84	1.70	1.79
MAE (OpL vs OBS)	3.51	2.48	1.09	1.88	0.95	0.96
5-day experiments for the summer (D01)						
Accumulated precipitation (OBS)	58	54	7	16	49	89
Accumulated precipitation (OpL)	77	66	102	81	17	10
MAE (DA vs OBS)	0.37	0.41	0.10	0.17	0.75	0.99
MAE (OpL vs OBS)	0.86	0.76	0.80	0.91	0.39	0.68
5-day experiments for the summer (D02)						
Accumulated precipitation (OBS)	52	60	17	62	10	108
Accumulated precipitation (OpL)	126	17	80	64	70	71
MAE (DA vs OBS)	0.54	0.33	0.19	0.53	0.07	0.73
MAE (OpL vs OBS)	1.17	0.60	0.60	0.87	0.64	1.07

precipitation within the top 10% of the reference data ($>30\,\mathrm{mm\,day^{-1}}$) and the highest modeling skill measured by MAE defined in Eq. (4); 2) sites D and E exhibit similar behavior as sites B and C, except that their accumulated precipitation is within the top 10% of the open-loop experiment ($>25\,\mathrm{mm\,day^{-1}}$); and 3) sites F and G exhibit accumulated precipitation within the top 10% of the reference data but exhibit the lowest modeling skill measured by MAE.

Figures 13b–e demonstrate that the downscaling approach effectively disaggregates 6-h winter precipitation to the hourly scale, particularly for the case that the open-loop experiment falsely forecasts heavy rainfall. At sites B–E, it can be seen that the time series of 4D-Var analyses are in closer agreement with the reference data than those of open-loop forecasts. For those time intervals in which the open-loop forecasts have intense rainfall but the reference data do not, the WRF 4D-Var significantly reduces overestimation of the open-loop forecast. We see similar behaviors at all sites, especially in time intervals 1500–2000 UTC at site B; 1400–1700 UTC at site C; 0000–0600 UTC at site D; and 1600–1800 UTC at site E.

Figures 13f and 13g show that the downscaling approach occasionally overestimates precipitation analyses when the rainfall patterns in the open-loop forecasts and reference data are drastically different. In some sense, the overestimation problem is related to issues previously discussed in section 3e. At these two sites, the WRF 4D-Var reproduces downscaled precipitation over the time intervals in which the open-loop forecasts are rainy and remains dry when the open-loop forecasts are dry. In other words, the 4D-Var assimilation only increases the rainfall estimates over those time intervals where the open-loop forecast is raining rather than reproducing rainfall temporal patterns similar to the reference data. For example, it can be seen that the behavior of hourly precipitation is different between the reference data and the open-loop forecasts within the second assimilation cycle (0700–1200 UTC). In this cycle, the reference data show moderate rain from 0700 to 0800 UTC, with rainfall effectively stopping at 0900 UTC; however, the open-loop experiment only forecasts a small amount of precipitation at 1000 UTC. Assimilating 6-h rainfall observations, the WRF 4D-Var algorithm apparently increases the volume of precipitation analysis during the time intervals in which the open-loop forecasts are raining. As a result, we can see that the precipitation intensities at 1000 UTC for the reference data, DA experiment, and open-loop experiment are 0, 14, and 2 mm, respectively. These findings suggest that the proposed dynamical downscaling approach may be less effective in those analysis cycles within which the observed rainfall exhibits strong intermittency.

2) TIME SERIES OF 5-DAY SUMMER EXPERIMENTS (36-KM RESOLUTION)

In the summer experiments, similar assimilation effects are found as discussed in the previous section, except the fact that the effect is more drastic. In other words, the 4D-Var analyses still outperform the open-loop forecasts in a temporal sense at the hourly scale. However, because the temporal patterns of open-loop forecasts and assimilated observations are typically very different during the summer, the assimilation results are not as good as the winter experiments in terms of the examined quality metrics. Figure 14a shows the accumulated precipitation during the 5-day summer experiments with the location of the six selected sites. Figures 14b–g show the hourly precipitation time series at each site with the corresponding statistics reported in Table 1. The selection criteria for the six sites are the same as section 3f(1), except that the top 10% of the

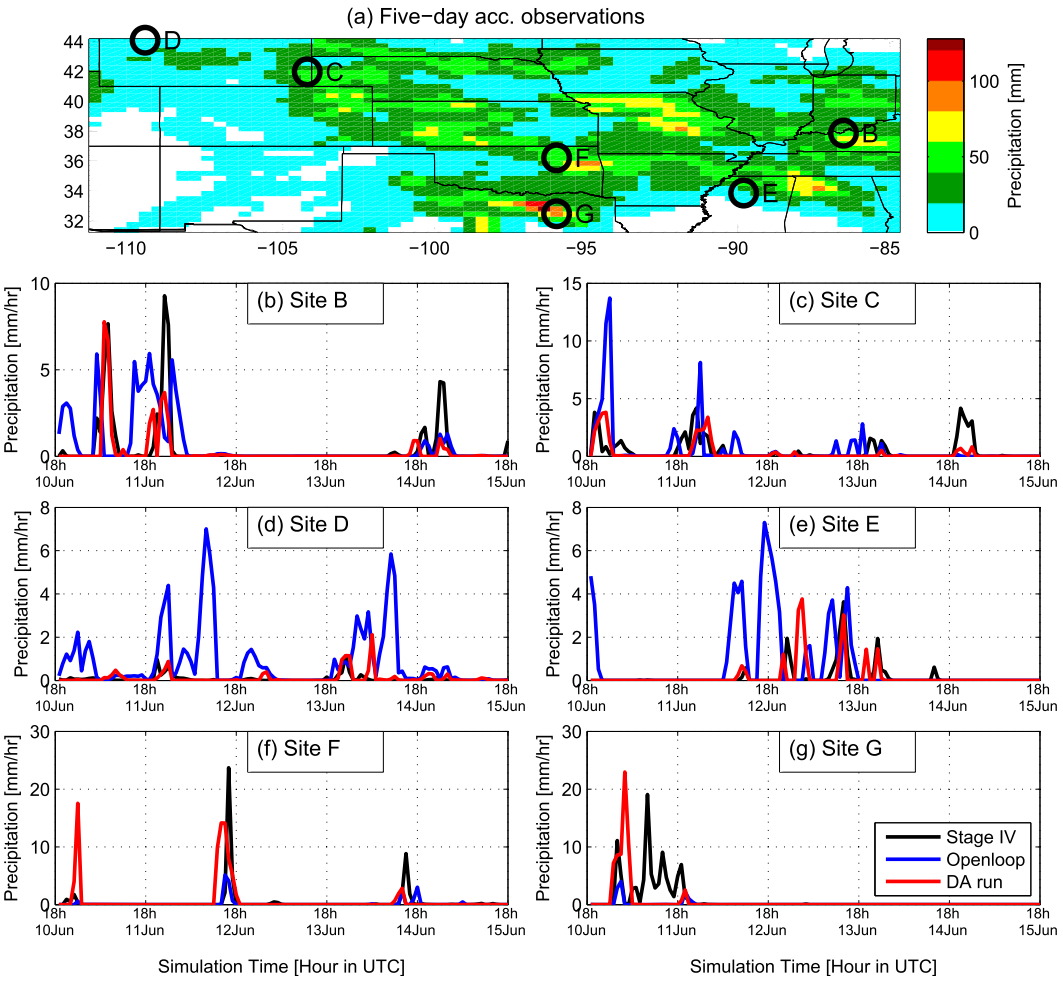

FIG. 14. As in Fig. 13, but for the outer domain (36-km resolution) of the summer experiments.

reference data and open-loop experiment are now 46 and 54 mm over 5 days, respectively. For sites B–E, it is clear that the DA was quite effective and improved the results of precipitation analyses with respect to the reference data compared to those of open-loop forecasts. On the other hand, the sites F and G show lowest downscaling performance. It can be seen that the DA experiment overestimates precipitation during very short periods of time, such as the hour 0000 UTC 11 June and the time interval from 1300 to 1800 UTC 12 June at site F, and underestimates from 0700 to 1800 UTC 11 June at site G. As discussed in section 3e, we suspect that the difficulty of precipitation downscaling is related to the imprecise forecast of summertime convective precipitation and the smoothing effect of the prescribed background error covariance.

3) TIME SERIES OF 5-DAY SUMMER EXPERIMENTS (9-KM RESOLUTION)

The hourly precipitation time series of six selected sites within the inner domain are also presented in Fig. 15 with the corresponding statistics reported in Table 1. The domain in Fig. 15a was divided into six regions, each containing a site with significant improvement measured by the MAE metric. Figures 15b–g demonstrate that in all cases the 4D-Var outperforms the open-loop experiment. However, both the open-loop forecasts and 4D-Var analyses occasionally missed high-intensity precipitation in the reference data (Fig. 15e). We can see that the assimilation scheme is fairly effective at reducing or removing rainfall intensities appearing in the open-loop forecasts that do not appear in the reference data. As a result, we conclude that our dynamical downscaling approach is sufficiently effective not only in improving precipitation accumulation measured by the described statistical metrics but also in precipitation estimation at hourly time and pixel scales.

4. Conclusions and future work

The WRF 4D-Var assimilation was examined for dynamical rainfall downscaling. We assimilated 6-h NCEP

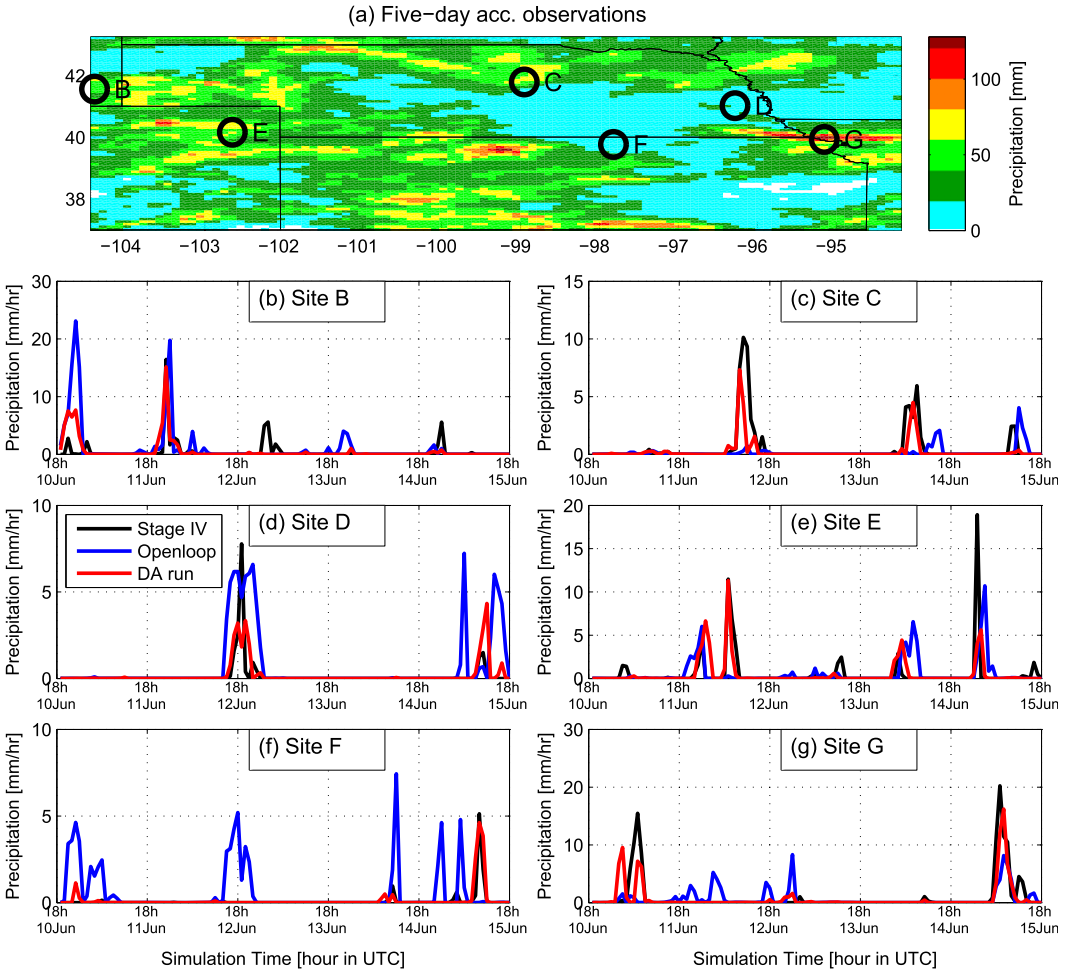

FIG. 15. As in Fig. 13, but for the inner domain (9-km resolution) of the summer experiments.

stage IV data at a gridded spatial resolution of 20 km into the WRF Model and compared the downscaled precipitation fields with hourly NCEP stage IV data at a gridded resolution of 9 km as a proof of concept. Precipitation data assimilation currently entails several major difficulties, such as the non-Gaussianity property of precipitation (Bauer et al. 2011a). Therefore, the overall success of our physically based downscaling experiment is promising for downscaling real GPM data to higher resolutions for hydrologic applications.

In summary, our point-scale assimilation experiment demonstrated that precipitation analysis might be very sensitive to direct rainfall assimilation. The results from both winter and summer experiments showed that the WRF 4D-Var system can effectively combine information from both observations and background states and use the underlying physics to produce hourly precipitation at the 9-km spatial resolution. In terms of the studied quantitative metrics, both winter and summer assimilation experiments over the outer domain (36-km resolution) indicated that using the built-in QCI can significantly improve the quality of the downscaled precipitation. In the seasonality comparison, we observed that the WRF forecasts are in closer agreement with the reference observations during the winter than those during the summer, and therefore, the downscaled precipitation analyses in the winter are in closer agreement with the reference data than those in the summer. We also observed that the WRF 4D-Var system is very effective in correcting forecast errors when open-loop forecasts falsely produce high-intensity rain cells over areas of no or light rainfall in the reference fields.

The proposed downscaling algorithm can be further studied from several perspectives for a broader understanding of the WRF 4D-Var precipitation DA. First, while we demonstrated promising results by assimilating stage IV rainfall data, future research needs to be devoted to the direct assimilation of GPM or TRMM products and the evaluation of the results. Second, additional case studies, over longer time periods, are essential for enhancing our

understanding of the longer-term and seasonal performance of the dynamical downscaling. Third, understanding the sensitivity of the proposed approach to the use of other global datasets (e.g., the ECMWF products) for the boundary conditions requires further investigation. Although we demonstrated the effectiveness of our proposed downscaling approach, two difficulties in downscaling summertime small-scale precipitation extremes need to be addressed in future research, including 1) ineffectiveness in reproducing heavy rain at pixels with non- or low-precipitation forecasts and 2) overestimation of convective cells. Instead of using time-invariant prescribed observational and background error covariance matrices and the subjective quality-control procedure, using a time-varying and adaptive error characterization scheme seems to be a promising area of future research. Moreover, to improve dynamical downscaling of convective precipitation, future research can be devoted to incorporating soil moisture data, a main driver of land surface turbulent heat fluxes (e.g., Chen et al. 2001; Case et al. 2011; Flores et al. 2012; Margulis et al. 2002; Peters-Lidard et al. 2011), into the proposed downscaling framework.

Acknowledgments. This research is sponsored by the NASA Precipitation Measurement Mission (PMM) science program through Grants NNX11AQ33G, NNX10AG84G, and NNX13AH35G; the NASA EPSCoR program through Grant NNX10AN30A; and the U.S. Army RDECOM ARL Army Research Office through Grants W911NF-09-1-0534 and W911NF-11-1-0310. The FNL data were provided by the Computational and Information Systems Laboratory at the National Center for Atmospheric Research (NCAR). The NCEP stage IV precipitation data were provided by the Earth Observing Laboratory at the NCAR. The WRF and WRFDA were obtained from the NCAR. The authors are grateful to these agencies for providing the models, data, and assistance.

REFERENCES

Barker, D., W. Huang, Y.-R. Guo, A. J. Bourgeois, and N. Xiao, 2004: A three-dimensional variational data assimilation system for MM5: Implementation and initial results. *Mon. Wea. Rev.,* **132,** 897–914, doi:10.1175/1520-0493(2004)132<0897:ATVDAS>2.0.CO;2.

——, and Coauthors, 2012: The Weather Research and Forecasting (WRF) Model's community variational/ensemble data assimilation system: WRFDA. *Bull. Amer. Meteor. Soc.,* **93,** 831–843, doi:10.1175/BAMS-D-11-00167.1.

Bauer, P., P. Lopez, D. Salmond, A. Benedetti, S. Saarinen, and M. Bonazzola, 2006a: Implementation of 1D+4D-Var assimilation of precipitation-affected microwave radiances at ECMWF. I 1D-Var. *Quart. J. Roy. Meteor. Soc.,* **132,** 2277–2306, doi:10.1256/qj.05.189.

——, ——, ——, ——, ——, and ——, 2006b: Implementation of 1D+4D-Var assimilation of precipitation-affected microwave radiances at ECMWF. II 4D-Var. *Quart. J. Roy. Meteor. Soc.,* **132,** 2307–2332, doi:10.1256/qj.06.07.

——, A. J. Geer, P. Lopez, and D. Salmond, 2010: Direct 4D-Var assimilation of all-sky radiances. Part I: Implementation. *Quart. J. Roy. Meteor. Soc.,* **136,** 1868–1885, doi:10.1002/qj.659.

——, G. Ohring, C. Kummerow, and T. Auligne, 2011a: Assimilating satellite observations of clouds and precipitation into NWP models. *Bull. Amer. Meteor. Soc.,* **92** (Suppl.), ES25–ES28, doi:10.1175/2011BAMS3182.1.

——, and Coauthors, 2011b: Satellite cloud and precipitation assimilation at operational NWP centres. *Quart. J. Roy. Meteor. Soc.,* **137,** 1934–1951, doi:10.1002/qj.905.

Case, J. L., S. V. Kumar, J. Srikishen, and G. J. Jedlovec, 2011: Improving numerical weather predictions of summertime precipitation over the southeastern United States through a high-resolution initialization of the surface state. *Wea. Forecasting,* **26,** 785–807, doi:10.1175/2011WAF2222455.1.

Chambon, P., S. Q. Zhang, A. Y. Hou, M. Zupanski, and S. Cheung, 2014: Assessing the impact of pre-GPM microwave precipitation observations in the Goddard WRF ensemble data assimilation system. *Quart. J. Roy. Meteor. Soc.,* **140,** 1219–1235, doi:10.1002/qj.2215.

Chen, F., and J. Dudhia, 2001: Coupling an advanced land surface–hydrology model with the Penn State–NCAR MM5 modeling system. Part I: model implementation and sensitivity. *Mon. Wea. Rev.,* **129,** 569–585, doi:10.1175/1520-0493(2001)129<0569:CAALSH>2.0.CO;2.

——, T. T. Warner, and K. Manning, 2001: Sensitivity of orographic moist convection to landscape variability: A study of the Buffalo Creek, Colorado, flash flood case of 1996. *J. Atmos. Sci.,* **58,** 3204–3223, doi:10.1175/1520-0469(2001)058<3204:SOOMCT>2.0.CO;2.

Dudhia, J., 1989: Numerical study of convection observed during the winter monsoon experiment using a mesoscale two-dimensional model. *J. Atmos. Sci.,* **46,** 3077–3107, doi:10.1175/1520-0469(1989)046<3077:NSOCOD>2.0.CO;2.

Flores, A. N., R. L. Bras, and D. Entekhabi, 2012: Hydrologic data assimilation with a hillslope-scale resolving model and L-band radar observations: Synthetic experiments with the ensemble Kalman filter. *Water Resour. Res.,* **48,** W08509, doi:10.1029/2011WR011500.

Fowler, H. J., S. Blenkinsop, and C. Tebaldi, 2007: Linking climate change modelling to impacts studies: Recent advances in downscaling techniques for hydrological modelling. *Int. J. Climatol.,* **27,** 1547–1578, doi:10.1002/joc.1556.

Geer, A. J., P. Bauer, and P. Lopez, 2010: Direct 4D-Var assimilation of all-sky radiances. Part II: Assessment. *Quart. J. Roy. Meteor. Soc.,* **136,** 1886–1905, doi:10.1002/qj.681.

Gutmann, E. D., R. M. Rasmussen, C. Liu, K. Ikeda, D. J. Gochis, M. P. Clark, J. Dudhia, and G. Thompson, 2012: A comparison of statistical and dynamical downscaling of winter precipitation over complex terrain. *J. Climate,* **25,** 262–281, doi:10.1175/2011JCLI4109.1.

Ha, J.-H., and D.-K. Lee, 2012: Effect of length scale tuning of background error in WRF-3DVAR system on assimilation of high-resolution surface data for heavy rainfall simulation. *Adv. Atmos. Sci.,* **29,** 1142–1158, doi:10.1007/s00376-012-1183-z.

——, H.-W. Kim, and D.-K. Lee, 2011: Observation and numerical simulations with radar and surface data assimilation for heavy rainfall over central Korea. *Adv. Atmos. Sci.,* **28,** 573–590, doi:10.1007/s00376-010-0035-y.

Hellstrom, C., D. Chen, C. Achberger, and J. Raisanen, 2001: Comparison of climate change scenarios for Sweden based on statistical and dynamical downscaling of monthly precipitation. *Climate Res.,* **19,** 45–55, doi:10.3354/cr019045.

Hong, S.-Y., J. Dudhia, and S. H. Chen, 2004: A revised approach to ice microphysical processes for the bulk parameterization of clouds and precipitation. *Mon. Wea. Rev.,* **132,** 103–120, doi:10.1175/1520-0493(2004)132<0103:ARATIM>2.0.CO;2.

——, Y. Noh, and J. Dudhia, 2006: A new vertical diffusion package with an explicit treatment of entrainment processes. *Mon. Wea. Rev.,* **134,** 2318–2341, doi:10.1175/MWR3199.1.

Hou, A. Y., G. Skofronick-Jackson, C. D. Kummerow, and J. M. Shepherd, 2008: Global precipitation measurement. *Precipitation: Advances in Measurement, Estimation, and Prediction,* S. Michaelides, Ed., Springer-Verlag, 131–169.

——, and Coauthors, 2014: The Global Precipitation Measurement Mission. *Bull. Amer. Meteor. Soc.,* **95,** 701–722, doi:10.1175/BAMS-D-13-00164.1.

Hsiao, L.-F., D.-S. Chen, Y.-H. Kuo, Y.-R. Guo, T.-C. Yeh, J.-S. Hong, C.-T. Fong, and C.-S. Lee, 2012: Application of WRF 3DVAR to operational typhoon prediction in Taiwan: Impact of outer loop and partial cycling approaches. *Wea. Forecasting,* **27,** 1249–1263, doi:10.1175/WAF-D-11-00131.1.

Huang, X.-Y., and Coauthors, 2009: Four-dimensional variational data assimilation for WRF: Formula and preliminary results. *Mon. Wea. Rev.,* **137,** 299–314, doi:10.1175/2008MWR2577.1.

Huffman, G. J., and Coauthors, 2007: The TRMM multisatellite precipitation analysis (TMPA): Quasi-global, multiyear, combined-sensor precipitation estimates at fine scales. *J. Hydrometeor.,* **8,** 38–55, doi:10.1175/JHM560.1.

Kain, J. S., and J. M. Fritsch, 1990: A one-dimensional entraining/detraining plume model and its application in convective parameterization. *J. Atmos. Sci.,* **47,** 2784–2802, doi:10.1175/1520-0469(1990)047<2784:AODEPM>2.0.CO;2.

Koizumi, K., Y. Ishikawa, and T. Tsuyuki, 2005: Assimilation of precipitation data to the JMA mesoscale model with a four-dimensional variational method and its impact on precipitation forecasts. *SOLA,* **1,** 45–48, doi:10.2151/sola.2005-013.

Lin, Y., and K. E. Mitchell, 2005: The NCEP stage II/IV hourly precipitation analyses: Development and applications. Preprints, *19th Conf on Hydrology,* San Diego, CA, Amer. Meteor. Soc., 1.2. [Available online at https://ams.confex.com/ams/pdfpapers/83847.pdf.]

Liu, Z., C. S. Schwartz, C. Snyder, and S. Ha, 2012: Impact of assimilating AMSU-A radiances on forecasts of 2008 Atlantic tropical cyclones initialized with a limited-area ensemble Kalman filter. *Mon. Wea. Rev.,* **140,** 4017–4034, doi:10.1175/MWR-D-12-00083.1.

Lopez, P., 2011: Direct 4D-Var assimilation of NCEP stage IV radar and gauge precipitation data at ECMWF. *Mon. Wea. Rev.,* **139,** 2098–2116, doi:10.1175/2010MWR3565.1.

——, and P. Bauer, 2007: "1D+4DVAR" assimilation of NCEP stage-IV radar and gauge hourly precipitation data at ECMWF. *Mon. Wea. Rev.,* **135,** 2506–2524, doi:10.1175/MWR3409.1.

Margulis, S. A., D. McLaughlin, D. Entekhabi, and S. Dunne, 2002: Land data assimilation and estimation of soil moisture using measurements from the Southern Great Plains 1997 field experiment. *Water Resour. Res.,* **38,** 1299, doi:10.1029/2001WR001114.

Mesinger, F., and Coauthors, 2006: North American Regional Reanalysis. *Bull. Amer. Meteor. Soc.,* **87,** 343–360, doi:10.1175/BAMS-87-3-343.

Mlawer, E., S. Taubman, P. Brown, M. Iacono, and S. Clough, 1997: Radiative transfer for inhomogeneous atmospheres: RRTM, a validated correlated-*k* model for the longwave. *J. Geophys. Res.,* **102,** 16 663–16 682, doi:10.1029/97JD00237.

Parrish, D. F., and J. C. Derber, 1992: The National Meteorological Center's spectral statistical-interpolation analysis system. *Mon. Wea. Rev.,* **120,** 1747–1763, doi:10.1175/1520-0493(1992)120<1747:TNMCSS>2.0.CO;2.

Peters-Lidard, C. D., S. V. Kumar, D. M. Mocko, and Y. Tian, 2011: Estimating evapotranspiration with land data assimilation systems. *Hydrol. Processes,* **25,** 3979–3992, doi:10.1002/hyp.8387.

Routray, A., U. C. Mohanty, D. Niyogi, S. R. H. Rizvi, and K. K. Osuri, 2010: Simulation of heavy rainfall events over Indian monsoon region using WRF-3DVAR data assimilation system. *Meteor. Atmos. Phys.,* **106,** 107–125, doi:10.1007/s00703-009-0054-3.

Schmidli, J., C. M. Goodess, C. Frei, M. R. Haylock, Y. Hundecha, J. Ribalaygua, and T. Schmith, 2007: Statistical and dynamical downscaling of precipitation: An evaluation and comparison of scenarios for the European Alps. *J. Geophys. Res.,* **112,** D04105, doi:10.1029/2005JD007026.

Schwartz, C. S., Z. Liu, Y. Chen, and X. Huang, 2012: Impact of assimilating microwave radiances with a limited-area ensemble data assimilation system on forecasts of typhoon Morakot. *Wea. Forecasting,* **27,** 424–437, doi:10.1175/WAF-D-11-00033.1.

Skamarock, W. C., and Coauthors, 2008: A description of the Advanced Research WRF version 3. NCAR Tech. Note NCAR/TN-475+STR, 113 pp., doi:10.5065/D68S4MVH.

Tsuyuki, T., 1996a: Variational data assimilation in the tropics using precipitation data. Part I: Column model. *Meteor. Atmos. Phys.,* **60,** 87–104, doi:10.1007/BF01029787.

——, 1996b: Variational data assimilation in the tropics using precipitation data. Part II: 3D model. *Mon. Wea. Rev.,* **124,** 2545–2561, doi:10.1175/1520-0493(1996)124<2545:VDAITT>2.0.CO;2.

——, 1997: Variational data assimilation in the tropics using precipitation data. Part III: Assimilation of SSM/I precipitation rates. *Mon. Wea. Rev.,* **125,** 1447–1464, doi:10.1175/1520-0493(1997)125<1447:VDAITT>2.0.CO;2.

Wang, H., J. Sun, X. Zhang, X.-Y. Huang, and T. Auligne, 2013: Radar data assimilation with WRF 4D-Var. Part I: System development and preliminary testing. *Mon. Wea. Rev.,* **141,** 2224–2244, doi:10.1175/MWR-D-12-00168.1.

Xu, J., and A. M. Powell, 2012: Dynamic downscaling precipitation over South Asia: Impact of radiance data assimilation on the forecasts of the WRF-ARW Model. *Atmos. Res.,* **111,** 90–113, doi:10.1016/j.atmosres.2012.03.005.

Zhang, S. Q., M. Zupanski, A. Y. Hou, X. Lin, and S. H. Cheung, 2013: Assimilation of precipitation-affected radiances in a cloud-resolving WRF ensemble data assimilation system. *Mon. Wea. Rev.,* **141,** 754–772, doi:10.1175/MWR-D-12-00055.1.

Zupanski, D., and F. Mesinger, 1995: Four-dimensional variational assimilation of precipitation data. *Mon. Wea. Rev.,* **123,** 1112–1127, doi:10.1175/1520-0493(1995)123<1112:FDVAOP>2.0.CO;2.

——, S. Q. Zhang, M. Zupanski, A. Y. Hou, and S. H. Cheung, 2011: A prototype WRF-based ensemble data assimilation system for dynamically downscaling satellite precipitation observations. *J. Hydrometeor.,* **12,** 118–134, doi:10.1175/2010JHM1271.1.